Comprehensive investigation of the photophysics and supramolecular organisation of Congo Red in solution, the solid state, and intercalated in a layered double hydroxide

Ana L. Costa,[a] Ana C. Gomes,[b] Martyn Pillinger,*[b] Isabel S. Gonçalves,[b] João Pina,[a] and J. Sérgio Seixas de Melo*[a]

Abstract: Steady-state and time-resolved absorption and fluorescence measurements are reported for Congo Red (CR) in aqueous and DMSO solutions. The very low fluorescence quantum yield (~10-4) for CR in dilute solutions together with the absence of a triplet state indicates that internal conversion is the dominant deactivation route with more than 99.99% of the quanta loss (attributed to the energy gap law). Although no direct evidence for trans-cis photoisomerization was obtained from absorption or fluorescence data, the global analysis of fs-transient absorption data indicates the presence of a photoproduct with a lifetime of ~170 ps that is suggested to be associated with such a process. Spectral data for more concentrated CR solutions indicate the presence of oblique or twisted J-type aggregates. These results are compared with spectra for CR in the solid-state (sodium salt) and intercalated in a layered double hydroxide via a one-step coprecipitation route. Powder XRD and electronic spectral data for the nanohybrid indicate that the CR guest molecules are intercalated as a monolayer consisting of slipped cofacial J-type aggregates.

1. Introduction

The non-covalent self-association of organic dyes in solution and in the solid-state is a critically important phenomenon that leads to the formation of dimers and higher ordered aggregates [1-4]. Internal (dye structure related) factors that are involved in aggregate formation include electrostatic interactions, van der Waals forces, π-π stacking, and hydrogen bonding. Aggregation behavior is also strongly affected by external (dye environment related) factors such as temperature, pH, concentration of the dye, ionic strength, and solvent polarity. One of the main consequences of the self-assembly of dyes is that molecular aggregates have distinct photophysical properties compared to the individual monomer [3-5]. In many cases the strong intermolecular interactions that hold aggregates together are responsible for the weakening of emission ("aggregation-caused quenching") and this may severely limit the use of the dyes in real-world applications such as organic light-emitting diodes (OLEDs) [6]. On the other hand, the fairly recent discovery of "aggregate-induced emission" (AIE), in which non-emissive luminogens are induced to emit by aggregate formation, has gone a long way to tempering the bad reputation of aggregation with respect to luminescence efficiencies [1,7]. Therefore, studies on controlling dye aggregate formation and morphology, and the formation mechanism of these aggregates in, for example, thin films and dye-based nanohybrids [8-12], are of great importance for practical applications as well as for fundamental research of assembled dye molecules.

The aggregation behavior of azobenzenes (ABs) [13] is of considerable interest with respect to applications in optics and photonics since these molecules exhibit attractive features such as vibrant, chemically tunable colors (especially red, orange and yellow) [14], good light fastness, an ability to undergo reversible *trans-cis* isomerization upon irradiation with UV or visible light [15], and, in a few cases, AIE enhancement [16]. Congo Red (CR) is an anionic diazo dye with a high self-assembling tendency. In aqueous solution, CR is thought to form supramolecular structures of various sizes and shapes (ribbon or rod-like micelles) owing to the hydrophobic interactions between the aromatic rings of the dye [17-21]. These molecular assemblies may play a role in the remarkable ability of CR to bind to various Amyloid-β (Aβ) peptide species ranging from monomers to fibrils [17,22,23]. In fact, the capacity of CR to inhibit Aβ aggregation has led to its study as a therapeutic agent for amyloid fibril-related diseases such as Alzheimer's disease [22]. Interestingly, CR exhibits enhanced fluorescence and/or induced optical activity (circular dichroism) when bound to amyloid fibrils [24,25], synthetic peptides [26], poly(L-lysine) [27], enzymes [28] and proteins [29]. CR readily forms complexes with other materials such as cellulose fibers [30], the polysaccharide grifolan [31], poly(vinyl alcohol) hydrogels [32], graphite oxide [33], and has been incorporated into polymer films and capsules [34-36]. Composite materials containing embedded CR molecules are potentially of interest as pH and chemical sensors [37-41], hybrid organic-semiconductor devices [42], photoresponsive materials [43], polymer-electrolyte fuel cells [44], and nanotheranostics systems [45].

In view of the fundamental and technological interest in organized assemblies of AB dyes like CR, and the desire for a "bottom-up" approach to the assembly of tailored molecular aggregates, it is vital to gain an in-depth knowledge of aggregation behavior and structure-property relationships for the dye molecules in different environments. Here, we report a comprehensive study of the electronic spectral and photophysical behavior of CR in solution and in the solid state as well as in the aggregated state in an organo-layered double hydroxide nanocomposite prepared by a direct coprecipitation route. In the latter case the photophysical characterization was

[a] A. L. Costa, Dr. J. Pina, Dr. J. S. Seixas de Melo
Coimbra Chemistry Centre, Department of Chemistry
University of Coimbra
Rua Larga, 3004-535 Coimbra, Portugal
E-mail: sseixas@ci.uc.pt (J. S. Seixas de Melo)
[b] Dr. A. C. Gomes, Dr. M. Pillinger, Dr. I. S. Gonçalves
Department of Chemistry, CICECO - Aveiro Institute of Materials
University of Aveiro
Campus Universitário de Santiago, 3810-193 Aveiro, Portugal
E-mail: mpillinger@ua.pt (M. Pillinger)

Supporting information for this article is available on the WWW under http://dx.doi.org/10.1002/cphc.2016xxxxx.

complemented by several other solid-state measurements in order to determine more precisely the structural properties of the intercalated dye aggregates.

2. Results and Discussion

2.1. CR in solution

2.1.1. Absorption, fluorescence and fluorescence excitation studies

Prior to the study of the compounds in the solid-state, the photophysical properties of CR were investigated in solution. UV-Vis absorption and steady-state fluorescence spectra of CR in aqueous solution were previously reported.[46] However, according to our results for as-received CR and recrystallized CR (Figure S1 in the Supporting Information), the emission spectra (and photophysical parameters) reported by Iwunze[46] originate from an impurity in the reagent-grade CR obtained from a commercial source (and used without further purification). Iwunze obtained a value of 0.011 for the fluorescence quantum yield (with excitation at 330 nm and observed fluorescence at 417 nm, in the $S_0 \rightarrow S_2$ transition) and determined the lifetime as 2.8 ns by using the Strickler-Berg equation.[47] As will be shown below the lifetime of the S_1 state is actually much shorter with a value of 7 ps. A similar excitation in the S_2 band (350 nm) for CR incorporated within a dendritic structure in ethanol, dichloromethane or pentane gave fluorescence emission spectra with maxima that ranged from 402 nm (polar solvent) to 632 (non-polar solvent), with this behavior being attributed mainly to aggregation induced by the nonpolar solvent.[48]

In the present study, the CR sample was purified by recrystallization and, although the absorption spectra recorded before and after purification were identical, the purification step led to a major change in the emission spectrum, namely the disappearance of the emission band at shorter wavelengths (Figure S1).

The absorption and fluorescence spectra of CR were measured in two solvents with different polarities, namely water, a polar protic solvent and a strong hydrogen-bond donor, and DMSO, a polar aprotic solvent with no ability to be a hydrogen-bond donor. The absorption spectra (Figure 1) display two broad bands with maxima at 340 and 497 nm in water (pH = 6.3), and at 340 and 532 nm in DMSO, assigned to π-π^* transitions of the –NH and azo groups, respectively.[49] CR, with high absorptivity, can undergo solvatochromic shifts depending on the dye-solvent interactions.[49] The negative solvatochromism evident in Fig. 1 is in agreement with results published previously by Atvars and co-workers.[30]

At the concentrations used to acquire the spectra shown in Figure 1 the solution behavior is plainly that of the isolated molecule, which has no parallel with the situation found with the CR-LDH hybrid (see below). In order to further support the type of aggregates formed by CR in CR-LDH we measured the absorption and emission excitation spectra of CR in DMSO and water from higher (2.64×10^{-4} M) to lower (2.64×10^{-6} M) concentrations (see Figure S2 for the absorption spectra at different concentrations and Figure 2 for the fluorescence excitation spectra). Typically, increasing dye concentration may induce molecular aggregation and cause spectral perturbation. Current interpretations of these effects have their historical roots in the exciton model introduced by Kasha[50,51] and have recently been (critically) reviewed.[3,52] Nearest neighbor interactions have the most significant effects on the UV-Vis spectrum of the molecular aggregate. Head-to-tail stacking of dyes leads to a red-shift in the absorption spectrum (J-aggregates), while a parallel stacking arrangement leads to a blue shift (H-aggregates).[52-55]

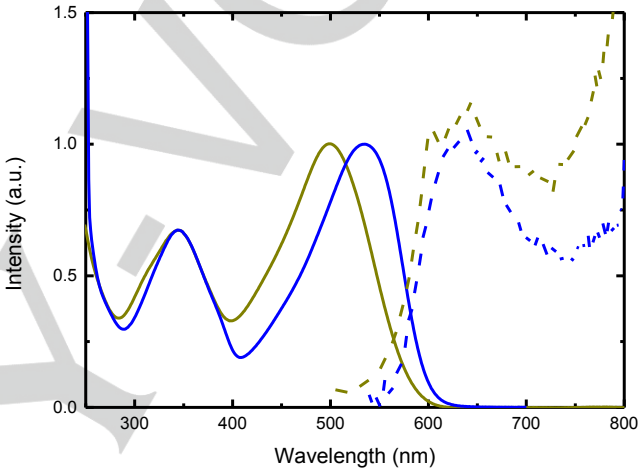

Figure 1. Absorption spectra (unbroken lines) of Na_2CR in water with C = 6.60×10^{-6} M (dark yellow) and in DMSO with C = 2.77×10^{-6} M (blue), and fluorescence emission spectra (dashed lines) of Na_2CR in water with λ_{exc} = 497 nm (dark yellow) and in DMSO with λ_{exc} = 535 nm (blue).

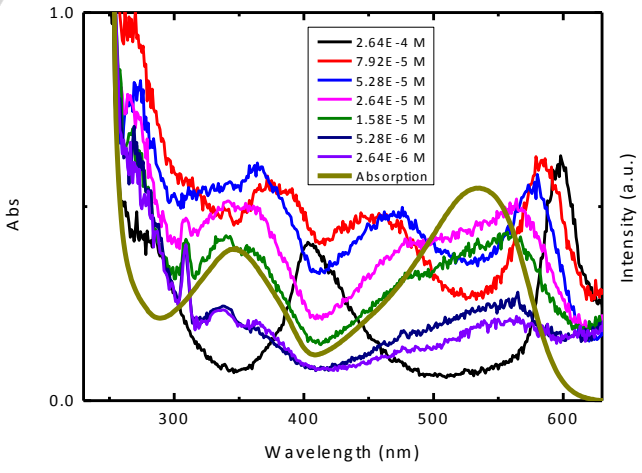

Figure 2. UV-Vis Absorption and excitation spectra (obtained with λ_{em}= 680 nm) in the 230-630 nm wavelength range for CR in DMSO at different concentrations.

For the absorption spectra of CR in DMSO, a linear dependence is observed within the concentration range studied (the saturation limit of the spectrophotometer is the limiting factor for this linear dependence). This means that the compound is very soluble (in DMSO and water). Nevertheless, the excitation spectra provide additional evidence for aggregation and the types of aggregates present in solution. Indeed, the fluorescence excitation spectra of CR in DMSO are different from the corresponding UV/Vis absorption spectra, particularly when the concentration is above 2.64×10^{-5} M. For concentrations in the range of 2.64×10^{-6} M to 1.58×10^{-5} M, the excitation spectra of CR can be considered identical to its absorption spectra with no appreciable change upon increase in the concentration (Figure 2). Within this concentration range the CR molecules can be considered as "isolated". When the concentration increases from 2.64×10^{-5} M to 7.92×10^{-5} M, a red-shift of the longest wavelength band, together with a significant change in the spectral shape (with a characteristically sharp absorption spectra) is observed, which indicates the presence of J-type aggregates. Moreover, at the final concentration of 2.64×10^{-4} M an additional, now blue-shifted band (at ~ 405 nm) is observed, which is consistent with the fact that with oblique-type aggregates there is an energetic split of the excited states leading to a splitting into two bands, which appear at low and high wavelengths in the absorption spectrum.[56,57] A similar situation is observed for the behavior in water as can be seen from the fluorescence excitation spectra obtained at different concentrations (Figure S3).

The fluorescence spectra present a broad band with maximum at 630 nm in water and 640 nm in DMSO (Figure 1). The fluorescence quantum yields were determined for both solvents and are presented in Table 1. From the very low fluorescence quantum yield values (ca. 10^{-4}) and the absence of a transient triplet-triplet signal (no signal was observed by nanosecond transient absorption flash-photolysis) it can be concluded that the main deactivation pathway in CR is the internal conversion radiationless channel. It is noteworthy that the ϕ_F value is ca. 2 times lower in water than in DMSO. These low ϕ_F values, together with the fact that CR presents a pH dependent photophysical behavior (see below), suggest *a priori* that excited state proton transfer (ESPT) may be responsible for the domination of the radiationless deactivation channel. Indeed, in water the possibility of intermolecular ESPT in addition to intramolecular ESPT seems to open up an additional (and effective) deactivation channel for CR, thus decreasing the ϕ_F value. This will be further discussed in the next section in the light of the femtosecond time-resolved transient absorption data (fs-TA). Since the decay of the first excited singlet state basically occurs through radiationless internal conversion, the fluorescence decay time can be considered to be identical to the overall decay time of this state. Thus, based on the decay time value of the S_1 obtained from fs-TA experiments, the radiationless rate constant (k_{NR}) dominates relative to the radiative processes in the excited state deactivation of CR in solution (more than five thousand times for water), see Table 1. In DMSO this domination is reduced markedly (ca. 400 times difference). Others have reported a value of 2.3 ns for the fluorescence lifetime of CR in ethanol.[48] However, as mentioned above and as shown in the present work, we believe that this is likely related to an impurity present in CR. Indeed, we have also obtained a value of 8.11 ns (degassed solution) for the fluorescence decay time of CR in DMSO when excited at 339 nm (S_2) for the impure compound (Figure S4).

Table 1. Spectroscopic and photophysical properties of Congo Red, including absorption and emission wavelength maxima, molar extinction coefficient ($\varepsilon_{máx}$), fluorescence quantum yield (ϕ_F), fluorescence lifetime (τ_F) and radiative (k_F) and radiationless (k_{NR}) rate constants , in water (pH = 6.10) and DMSO, at room temperature.[a]

Solvent	λ_{max}^{Abs} (nm)	$\varepsilon_{máx}$ (mol dm^{-3} cm^{-1})	λ_{max}^{Fluo} (nm)	ϕ_F[b]	τ_F (ns)[b]	k_F (ns^{-1})	k_{NR} (ns^{-1})
Water	340, 497	37410	630	1.9×10^{-4}	0.0062	0.0306	161.26
DMSO	340, 532	45500	640	3.8×10^{-4}	0.0075	0.0507	19.73

[a] For the fluorescence quantum yields (ϕ_F) and fluorescence lifetimes (τ_F) the excitation was made in $S_0\rightarrow S_1$ band.

[b] Associated errors are ± 3.5×10^{-5} for water and ± 1.8×10^{-5} for DMSO. [b] Obtained from fs-TA experiments, considering that the dominating deactivation of the S_1 state does not involve the formation of a triplet state.

As mentioned in the introduction, cis-trans photoisomerization of azo-dyes is usually a dominant process in the excited state. However, in our case for CR in solution, only photodegradation was observed upon irradiation. This contrasts with previous observations for composite films of PDAC and CR where photoisomerization of CR was found together with degradation (with an Ar^+ laser with an intensity of 100 mW/cm^2 and excitation at 488 nm).[35]

Recently, a theoretical study on an azo-derivative (cyclopropyldiazo-2-naphthol) suggested an ESPT (wavelength-dependent) could be present.[58] Although we cannot completely exclude the possibility of ESPT, the very low fluorescent quantum yields together with the high values (and dominance) of the radiationless rate constants (k_{NR}) seem to be better explained by the energy gap law for the radiationless transitions. In this case a small value in the S_1-S_0 energy gap, ΔE, as observed in the case of CR, favors the nonradiative vs radiative decay pathway. This is limited by the degree of vibrational overlap (Franck-Condon factor, f_v) of the wavefunctions for the nonradiative modes of these two states. This is linked to the fact that the changes in the f_v factors of the nuclear wavefunctions become increasingly unfavorable with the increase in the energy separation between the two states.[59,60] Indeed if we consider that the rate constant for internal conversion $k_{IC}\sim10^{13}\ f_v\ s^{-1}$ and $k_{IC}\sim10^{13}\exp(-\alpha\Delta E)$, where α is a proportionality constant, the f_v value becomes largely unfavorable with the increase in ΔE.[60] In our case, considering that intersystem crossing ($S_1\sim\sim>T_1$) is a negligible excited state deactivation pathway, we can assume

that k_{NR}~ k_{IC}. Thus the values of 1.613×10^{12} s^{-1} (water) and 1.97×10^{12} s^{-1} (DMSO), see Table 1, are close to the limiting value for the rate of internal conversion (10^{13} s^{-1}).[60]

Figure 3 shows the evolution of the absorption spectra of an aqueous solution of Na_2CR as a function of pH. The color of the solution changes from blue for acidic solutions to red at higher pH values.[30,49] It has been proposed that for pH values above 5.6 the disulfonate dianion of CR is present and gives rise to the band at 497 nm. Below a pH of 5.6, spectral changes are due to the protonation of CR and the existence of a tautomeric equilibrium mixture comprising an ammonium form (λ_{max} = 520 nm) with the proton attached to the amino nitrogen and an azonium form (λ_{max} = 655 and 735 nm) with the proton attached to the α-azo nitrogen.[61] For pH values below 1.96, there is a tendency for CR to precipitate, which results in a decrease in the absorbance.

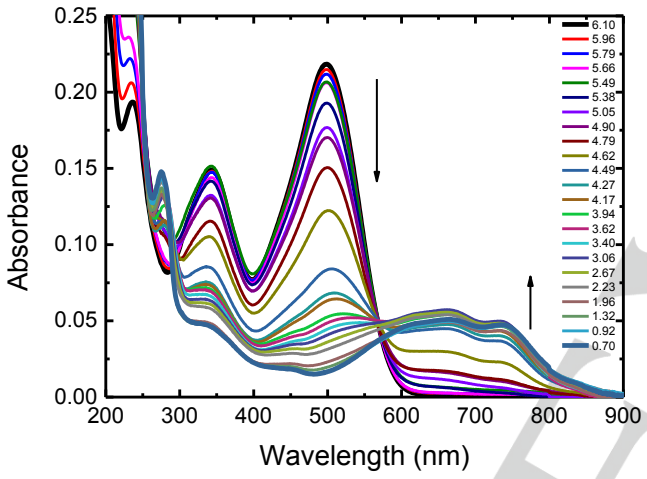

Figure 3. Absorption spectra of an aqueous solution of Na_2CR (C = 5.83×10^{-6} M) as a function of pH.

2.1.2. Femtosecond transient absorption experiments

The transient absorption (TA) spectra for CR were obtained in aerated water and DMSO solutions at room temperature from pump-probe femtosecond time-resolved TA spectroscopy. The compounds were excited at 440 nm and 568 nm (pump light), thus promoting the population of the excited state, followed by an analysis/probing with light in the 450–800 nm range and recording the evolution of the TA spectra and decay kinetics up to a delay time of 50 ps.

Figure 4 depicts the ultrafast time-resolved TA spectra of CR in water at pH=10 and DMSO with excitation at 440 nm. In general in water and DMSO the spectra present a negative band ranging from ~400 nm to ~570 nm that is attributed to ground state bleaching (GSB), matching well the ground-state absorption peak, together with a positive excited state absorption (ESA) band in the 550-750 nm range. In water when excitation was made at 568 nm (0-0 transition band), similar TA spectra were obtained to that found with excitation at 440 nm, although in the latter case the ESA band appears more well defined, see Figures 4 and S5. In general, the ultrafast TA spectra do not display stimulated emission data, which may be explained by the very low fluorescence quantum yield found for CR (Table 1).

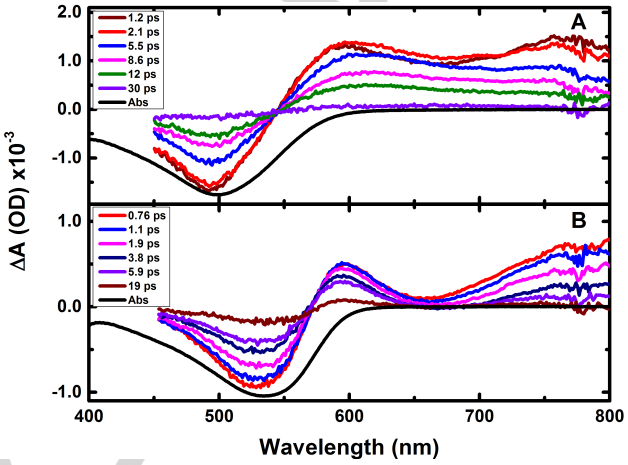

Figure 4. Ultrafast time-resolved TA spectra for CR in (A) water at pH=10 and (B) DMSO collected with excitation at 440 nm. For comparison the absorption spectra ($S_0 \rightarrow S_1$) obtained from UV-Vis spectroscopy are also shown.

At pH 10, and excitation at 440 nm and 568 nm, the individual analysis gives rise to a biexponential fit with decay times of 1.1-1.4 and 7.2-8.2 ps (data analysis not displayed). However, to describe properly the observed dynamics, global fit analysis of all of the kinetics at different wavelength regions was performed with singular value decomposition (SVD).[Please insert reference [83] J.J. Snellenburg, S.P. Laptenok, R. Seger, K.M. Mullen, I.H.M. van Stokkum, J. Stat. Soft. 2012, 49, 1-22.] A sequential kinetic model was used in the global analysis of the time-resolved data. The resultant decay-associated spectra, DAS, for CR in water at pH= 10 and DMSO are shown in Figure 5. The best-fits to the kinetic traces together with the evaluation of the quality of the fits can be found in Table 2 and Figure 5 (C, D), respectively.

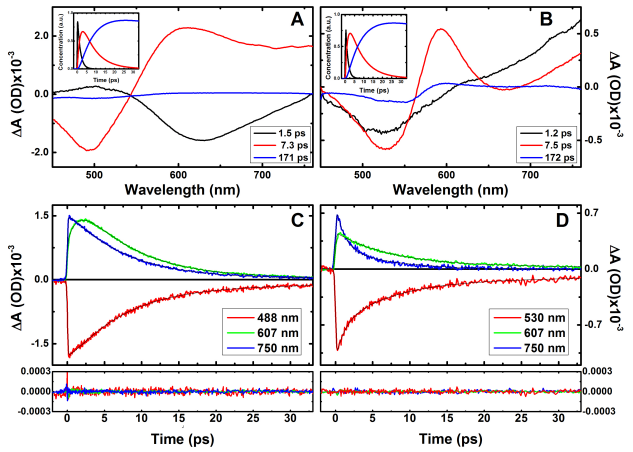

Figure 5. Decay associated spectra (DAS) of the three time constants extracted from the TA data (λ_{exc}= 440 nm) after SVD/global analysis together with the concentration profiles of the time constants (inset) for CR in (A) water at pH=10 and (B) DMSO; Representative kinetic traces of the TA data for CR in (C) water at pH=10 and (D) DMSO together with the fits derived from global analysis over the full 450-760 nm spectral range. The residuals are also presented for a better judgment of the quality of the fits.

Table 2. Results of the global fit analysis (lifetimes and normalized pre-exponential factors) for CR in water (pH = 10) and DMSO obtained from fs-TA experiments with λ_{exc} = 440 nm.

Solvent	λ (nm)	τ_1 (ps)	A_1	τ_2(ps)	A_2	τ_3(ps)	A_3
Water (pH = 10)	600	1.5	-0.59	7.3	0.98	171	0.02
	750		-0.10				
DMSO	600	1.2	-0.10	7.5	0.94	172	0.06
	750		0.66		0.34		-0.01

The results of the global analysis show that in general a better fit is obtained with a tri-exponential decay law. The two shorter components (1.2-1.5 ps and 7.3-7.5) are basically identical to the values obtained with the individual analysis. However, the lifetime value of ~170 ps and the residual associated pre-exponential factors (see Table 2 and the DAS in Figure 5) suggest that this component may result from the formation of a photoproduct; nevertheless it constitutes a minor route of CR decay dynamics.

Regarding the nature of the shorter decay component the fact that similar lifetime values were observed when excitation is made at 440 nm and 568 nm (0-0), excludes the occurrence of fast vibrational relaxation processes (due to vibrational cooling to the lowest vibronic state of S_1); indeed this component is more likely to be associated with the solvation dynamics process of water molecules (or DMSO) around the excited CR.[62]

Overall the data is consistent with a sequential model where upon excitation with a short laser pulse (≤250 fs) the excited state (Franck-Condon) is formed instantaneously in the excited state which further gives rise (with 1-2 ps) to a relaxed species that decays with 7.3-7.5 ps (this range is dependent on the solvent and pH). In our case the short component should be considered to include both the initial, very rapid, relaxation (also known as inertial solvation of water molecules around the excited CR molecule), essentially complete within ~1 ps, and the subsequent longer (diffusional component of the solvation) relaxation.[63]

It is worth discussing in more detail the data obtained with λ_{exc}=440 nm for CR in DMSO. Contrasting to the observation that at the band with maxima at ~596 nm and 750 nm (ESA) the kinetic trace completely decays, the decays in the GSB (530) do not completely recover. This is consistent with the formation of a long-lived (~170 ps) photoproduct (see Figure 5, A and B), which can be associated with a low degree of trans-cis photoisomerization.

2.2. CR in the solid-state

A Zn-Al LDH intercalated by Congo Red was prepared by coprecipitation of the Zn^{2+} and Al^{3+} hydroxides (initial Zn^{2+}/Al^{3+} molar ratio = 2) in the presence of an aqueous solution of the CR disodium salt at a constant pH of 7.5–8, followed by aging of the gel at 65 °C for 18 h. The PXRD pattern of the resultant dark red solid, denoted CR-LDH, exhibits several fairly broad, equally spaced peaks between 3 and 30º 2θ, which can be indexed as 00*l* reflections for an expanded hydrotalcite-type phase with a basal spacing (d_{003}) of 26.2 Å (Figure 6). This spacing is one of the largest yet reported for an LDH intercalated by an organic dye, surpassing that found for the azobenzenes methyl orange (24.2 Å).[64] (4-phenylazophenyl)acetate (25.6 Å),[65] and *trans*-azobenzene-4,4'-dicarboxylate (20.0 Å).[66] Relatively weak and asymmetric peaks above 30º 2θ are assigned as overlapping non-basal reflections. Subtraction of 4.8 Å (for the brucite-like layer thickness) from the basal spacing gives a gallery height of 21.4 Å. For comparison, Figure 6 shows the PXRD pattern of a nitrate-form Zn-Al LDH, which was prepared in a similar fashion to that for CR-LDH; as expected the basal spacing for NO_3-LDH (8.95 Å) is much lower than that for CR-LDH.

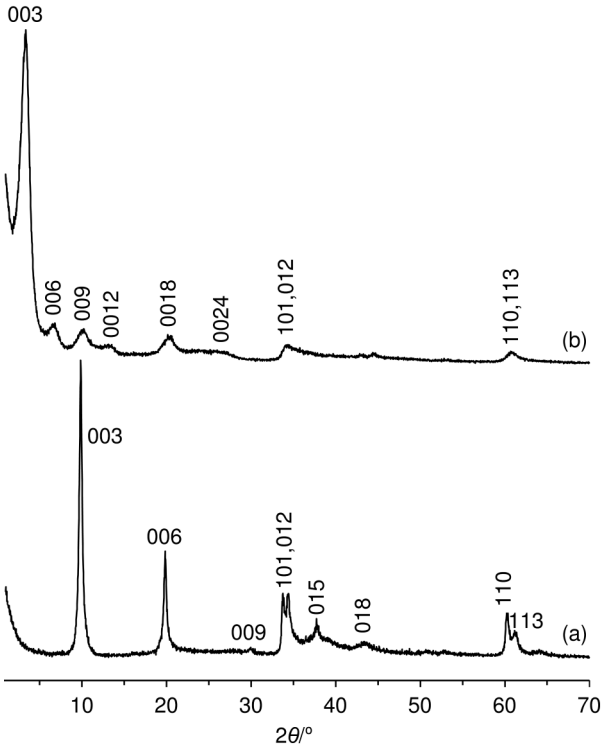

Figure 6. PXRD patterns of (a) NO_3-LDH and (b) CR-LDH.

The crystal structure of the calcium salt of CR was described by Gleason et al. in 1995.[67] Based on the reported data, the minimum and maximum dimensions of the CR anion can be represented by a rectangle with dimensions of 9.9 × 28.2 Å (which include van der Waals radii of 1.5 Å for oxygen and 1.2 Å for hydrogen, respectively). Hence, a perpendicular orientation of guest molecules between the layers is not compatible with the observed gallery height. However, a tilted arrangement with the molecules inclined at an angle of ca. 50º with respect to the LDH layers could account for the observed interlayer spacing, as illustrated schematically in Figure 7. Two different families (or extremes) of stacking arrangements can be envisaged based on whether the planes of the aromatic rings are in a roughly perpendicular (Figure 7a) or flat/parallel (Figure 7b) orientation with respect to the LDH layer. CR is known to self-assemble and create supramolecular structures in water solutions.[17] At low concentrations ($<10^{-5}$ M) and pH values higher than 5.5, CR possibly exists mainly as isolated molecules[26,30,34] and/or as small clusters composed of a few molecules.[20] At higher concentrations and/or lower pH values (where the amino groups are protonated, leading to a neutralization of electrostatic repulsive interactions between CR molecules) ribbon-shaped micellar species are created by the face-to-face stacking of CR molecules.[17,18,19,21] A similar type of supramolecular arrangement may be present in the intercalated material CR-LDH, as represented in Figure 7a. This type of face-to-face arrangement can be classified as a H-type aggregate and has been proposed for a number of dye-intercalated materials such as LDHs containing Acid Red 27[68] and 9-fluorenone-2,7-dicarboxylate.[69] By rotating/twisting each CR molecule in this model by ca. 90º along the molecular axis we arrive at the alternative model represented in Figure 7b in which the CR molecules are stacked in a slipped coplanar inclined configuration. The slip angle α (as defined in Figure 7b) is ca. 50º in this model, which is in the range (0-54.7º) conventionally associated with J-type aggregates (as opposed to H-type aggregates with α > 54.7º).[3,70] Examples of organic chromophores that have been proposed to adopt this type of guest packing when intercalated in LDHs include perylene derivatives,[71,72] 1,3,6,8-pyrenetetrasulfonate,[73] and indigo carmine.[74]

In the idealized representations shown in Figure 7a and 7b all of the CR molecules are drawn such that they have the same relative orientation, i.e. they are translationally equivalent. The actual situation may be more complex and modifications of this scheme can be envisaged in which adjacent coplanar CR molecules are twisted with respect to one another to varying degrees (while maintaining coplanarity). In the extreme (successive 180º rotations) the molecules would adopt an antiparallel arrangement, which has been proposed to be the most stable/favorable configuration for the above-mentioned CR mesophases in water, probably because it avoids close contact between the sulfonate groups of neighboring molecules.[18]

The type(s) of guest packing (H- or J-aggregates, or possibly even a mixture of the two as reported previously for perylene tetracarboxylate intercalated in a LDH[72]) present in the material CR-LDH cannot be unambiguously determined from the powder XRD data alone. However, as will be discussed below, the absorption spectrum for CR-LDH points to the prevalence of J-type aggregates. This is further substantiated by the excitation spectra obtained for different concentrations of CR in DMSO solution, where the progressive increase in concentration leads to the appearance of two bands (one sharp at λ>600 nm) at longer and shorter wavelengths, as will be discussed below.

Sun and co-workers studied the intercalation (by ion-exchange) of CR into arachidic acid/LDH hybrid films and concluded that the CR molecules formed head-to-tail J-type aggregates with a tilt angle of 31º with respect to the sheet surface (estimated from polarized UV-Vis absorption spectra and low-angle XRD).[75] This near-horizontal (parallel to the layers) arrangement is markedly different from the inclined (tilt angle of ca. 50º) orientation proposed here for the J-aggregate present in CR-LDH.

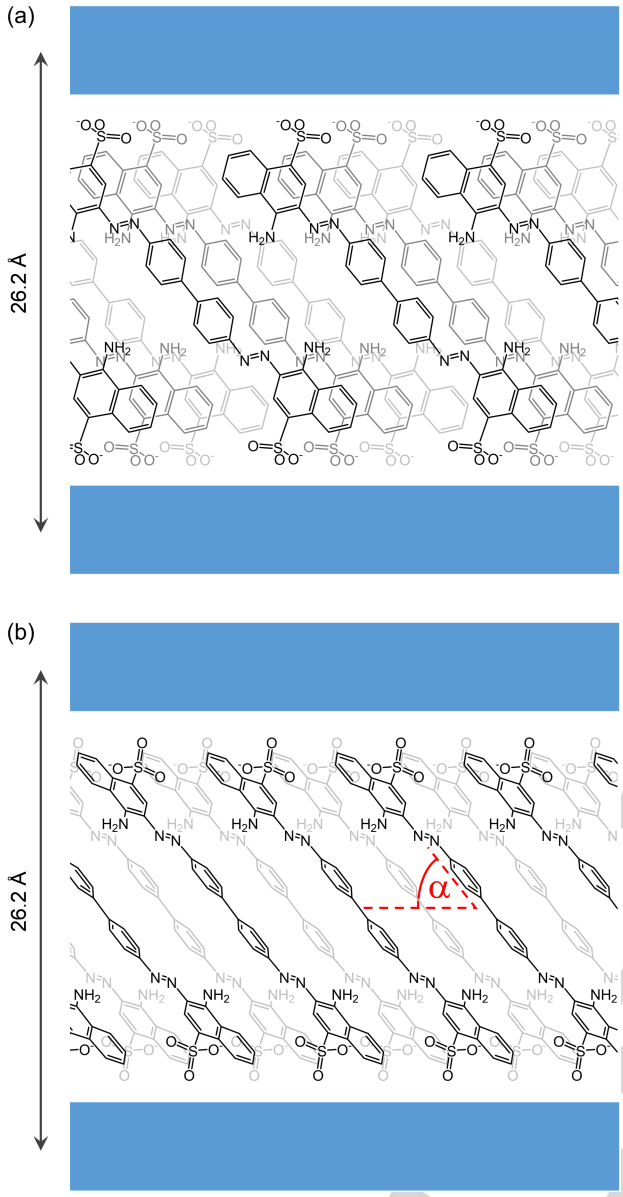

Figure 7. Schematic representation of possible arrangements for CR anions between the brucite-like layers in the material CR-LDH: (a) Face-to-face alignment, which allows an optimum interaction between sulfonate groups and the host layers, (b) slipped coplanar inclined alignment.

Scanning electron microscopy (SEM) studies showed that the morphology of the sample CR-LDH consisted of irregular aggregates of platelike particles (Figure 8).

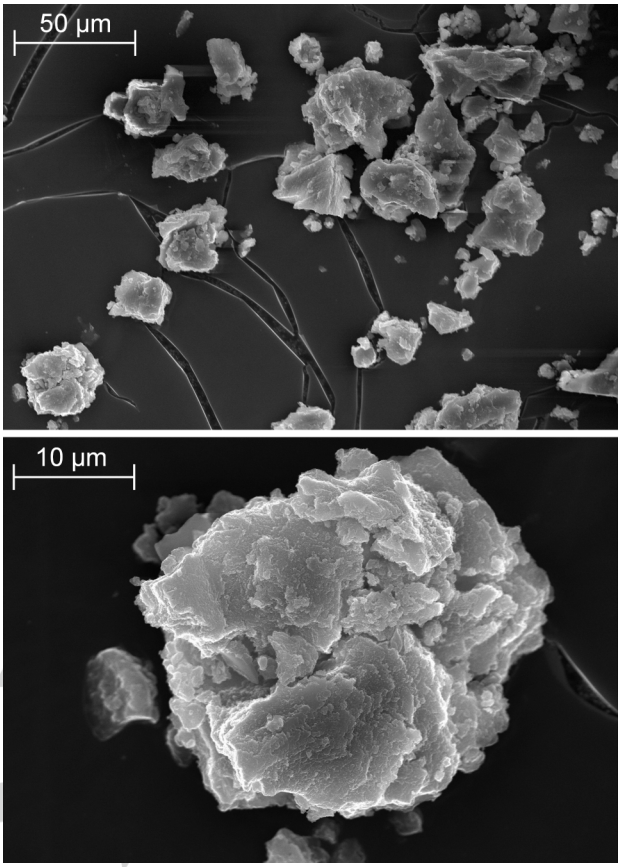

Figure 8. Representative SEM image of CR-LDH at two different magnifications.

Thermogravimetric analysis (TGA) revealed a 10.2% mass loss from ambient temperature up to 200 ºC, attributed to removal of interlayer water molecules, followed by a further loss of 7.4% up to 350 ºC (DTG_{max} = 275 ºC), attributed to dehydroxylation of the hydroxide layers (Figure 9). Decomposition of intercalated CR anions takes place in the interval 350-670 ºC (44.8% mass loss in two overlapping steps with DTG_{max} = 510 and 560 ºC). The composition of CR-LDH as deduced from elemental analysis (C, H, N and S) and thermogravimetry (water content) is $[Zn_4Al_2(OH)_{12}][(CR)_{0.86}(CO_3)_{0.14}(H_2O)_7]$. The CR content indicates that the anionic dye in effect balances about 86% of the positive charge of the hydroxide layers. In the proposed composition, carbonate anions counterbalance the remaining 14%. However, as described below, the IR spectrum of CR-LDH does not support the presence of significant amounts of carbonate (or nitrate) ions. Hence, the carbonate content may be less than that represented by the above composition. As proposed previously for composites of perylene bisimide dyes and LDHs,[71] it is possible that part of the residual positive charge is counterbalanced by hydroxide anions, i.e., the sample may contain a minor amount of a Zn-Al-OH phase.

The material CR-LDH was further characterized by spectroscopic techniques to confirm the presence of structurally

intact CR anions. The $^{13}C\{^1H\}$ MAS NMR spectra of CR-LDH and the CR disodium salt (Figure 10) match very well and exhibit four broad peaks at about 115 (C^6), 125 ($C^{2,3,5,7\text{-}9,11\text{-}14}$), 138 ($C^{4,10}$) and 150 ($C^1$) ppm.

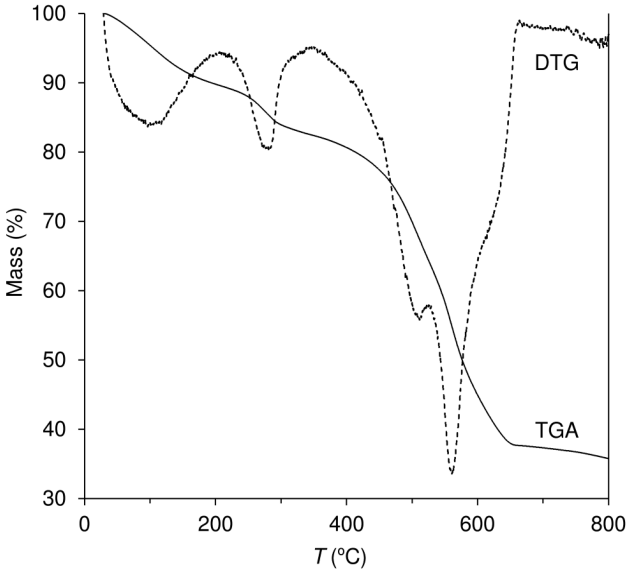

Figure 9. TGA curve and corresponding DTG trace of CR-LDH.

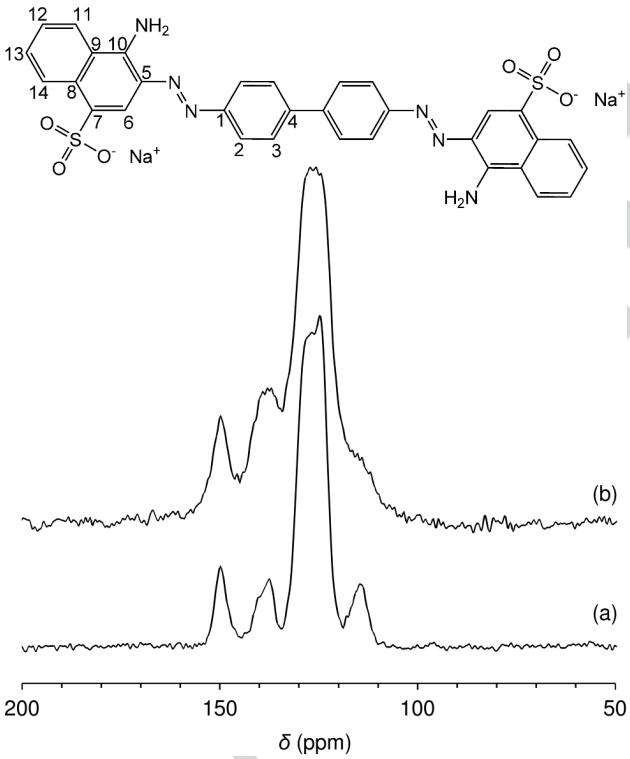

Figure 10. $^{13}C\{^1H\}$ MAS NMR spectra of (a) the disodium salt of CR and (b) CR-LDH. Chemical structure of the Congo Red molecule, showing the numbering scheme for the ^{13}C NMR assignments.

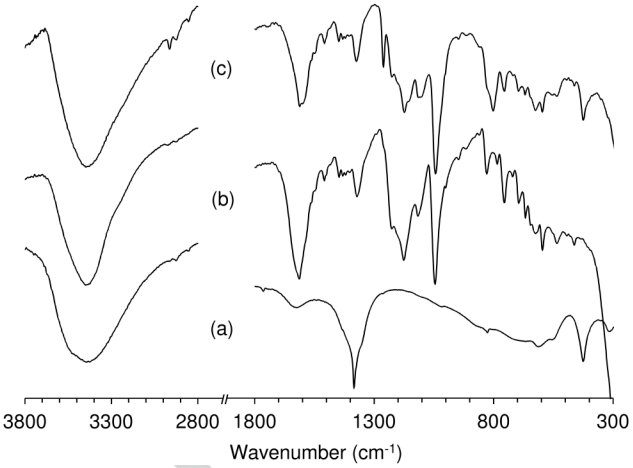

Figure 11. Selected regions of the FT-IR spectra of (a) NO_3-LDH, (b) Na_2CR and (c) CR-LDH.

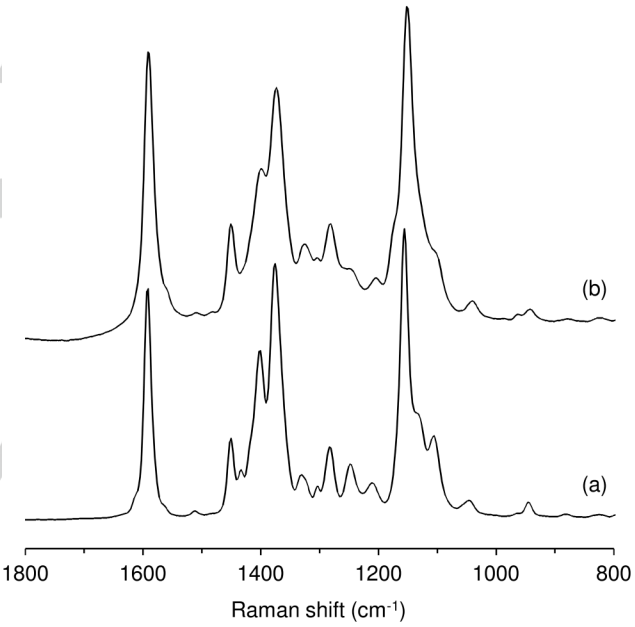

Figure 12. FT-Raman spectra in the range of 800-1800 cm^{-1} for (a) the sodium salt of CR and (b) CR-LDH.

As shown in Figures 11 and 12, the FT-IR and FT-Raman spectra of CR-LDH in the range 300-1800 cm^{-1} are dominated by bands due to the intercalated chromophore. In general, the bands are coincident with those displayed by the CR disodium salt, with only minor frequency shifts being observed. In the FT-IR spectrum of CR-LDH, the absorption bands for the asymmetric and symmetric stretching vibrations of the sulfonate group appear at 1174 and 1043 cm^{-1}, respectively, which are essentially unshifted when compared with those for Na_2CR (1176, 1045 cm^{-1}). Similarly, towards higher frequency, both Na_2CR and CR-LDH exhibit a broad band at 1612 cm^{-1} and a weak band at 1508 cm^{-1}, which are assigned to the aromatic

ring C–C stretching vibrations.[35] Near-identical frequencies for these vibrations were reported by Tripathy and co-workers for a multilayer composite film of a polyelectrolyte, poly(dimethyl diallylammonium chloride) (PDAC), and CR.[35] As mentioned above, no bands characteristic of either carbonate [$\nu_3(CO_3^{2-})$ at 1365 cm^{-1}] or nitrate [$\nu_3(NO_3^-)$ at 1383 cm^{-1}] are present in the IR spectrum of CR-LDH. The Raman spectra of Na_2CR and CR-LDH are very similar in the range of 800-1800 cm^{-1} (Figure 12). Bands at 1156 (phenyl-N= stretching mode), 1376 (naphthyl ring C–C stretching mode), 1401, 1451 (–N=N– stretching), and 1592 cm^{-1} (phenyl ring C–C stretching mode) for the salt Na_2CR are all present for CR-LDH. Of these, only the phenyl-N= stretching mode shifts by more than 2 cm^{-1} (5 cm^{-1} to lower frequency) upon intercalation of the dye molecule. In summary, the vibrational spectra confirm the successful intercalation of structurally intact CR anions in the composite CR-LDH. The data do not reveal any configurational change of the azo group (trans-cis isomerization) upon formation of CR-LDH.[76]

The absorption and fluorescence spectra recorded in the solid-state for CR-LDH and the CR disodium salt are compared in Figure 13 with the solution spectra obtained for Na_2CR in water and in DMSO. The spectrum for CR-LDH is red-shifted relative to both of the solution spectra, which is a direct consequence of the different electrostatic interactions present between the dye and the inorganic layers in the host-guest compound. Comparison of the solid-state spectra for Na_2CR and CR-LDH reveals the appearance of a shoulder at ~700 nm for the latter, which indicates the formation of J-type aggregates, according to exciton theory.[51,77] The intermolecular π-π interaction involving the conjugated ring system of the azo dye CR is the driving force for the formation of slipped cofacial J-type aggregates of CR.[35]

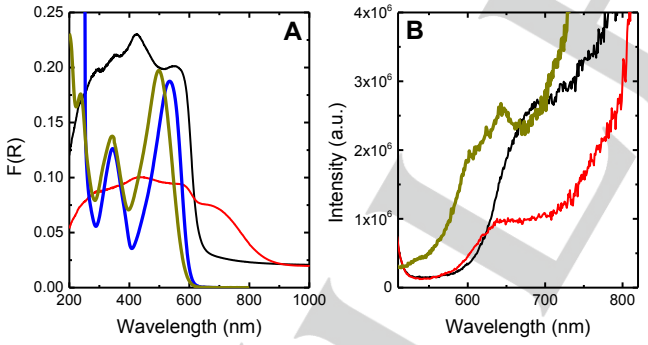

Figure 13. (**A**) Diffuse reflectance spectra (Kubelka-Munk scale) in the range of 200-1000 nm for Na_2CR in the solid-state (black), CR-LDH (red), Na_2CR in DMSO with C = 4.12×10^{-6} M (blue) and Na_2CR in water with C = 5.27×10^{-6} M (dark yellow). (**B**) Fluorescence emission spectra (λ_{exc} = 497 nm) of Na_2CR in the solid-state (black), CR-LDH (red) and Na_2CR in water with C = 5.27×10^{-6} M (dark yellow).

The fluorescence emission spectrum of the CR disodium salt in the solid state shows a broad band at 685 nm. Upon incorporation of CR in the LDH to give the composite material CR-LDH, the band (although broad) blue-shifts to 640 nm (Fig. 13B). However, it is interesting to note that for both the CR disodium salt in the solid state and the LDH, the emission spectra are red-shifted relative to the solution spectra (more so in the case of CR in the solid state), which seems to be in line with the preferential formation of J-type aggregates. Due to the very low fluorescence of CR, it was not possible to measure reliable quantum yields and time-resolved parameters for Na_2CR and CR-LDH in the solid-state.

3. Conclusions

In this paper we provide new insights into the photophysical properties of Congo Red (CR) in solution and have successfully demonstrated that the anionic dye can be incorporated into a layered double hydroxide by the direct coprecipitation method. From the photophysical studies it is shown that the solution behavior of CR is consistent with the formation of an excited species that decays with ~7 ps mainly through the radiationless internal conversion channel. In DMSO and for concentrations above ca. 3×10^{-5} M the fluorescence excitation spectra support the formation of oblique or twisted J-type aggregates of the dye. The characterization data for the CR-LDH intercalation compound suggest that a similar type of slipped cofacial J-type aggregate of the dye is assembled within the interlayer region, giving rise to the large basal spacing of 26.2 Å. This arrangement is different from the rod-like or ribbon-like supramolecular dye structures proposed in the literature for CR in aqueous solutions, which are built up from the face-to-face stacking (with zero or very small offset) of CR molecules. In the present case, a different binding force, namely the host-guest electrostatic interaction, is operative in addition to the water-dye and dye-dye interactions.

Experimental Section

General instrumentation

Elemental analysis for C, H, N and S was performed at the University of Aveiro with a Leco TruSpec 630-200-200 analyzer. PXRD patterns were recorded in transmission mode using a Philips Analytical Empyrean ($\theta/2\theta$) diffractometer equipped with a PIXcel1D detector, with automatic data acquisition (X'Pert Data Collector v4.2 software) and monochromatized Cu-K_α radiation (λ = 1.5406 Å). Each sample was mounted between two Mylar foils and then placed in the sample holder. The samples were step-scanned with 0.02º 2θ steps and a counting time of 50 s per step. Scanning electron microscopy (SEM) images were collected using a Hitachi SU-70 microscope operating at 15 kV. Samples were prepared by deposition on aluminium sample holders followed by carbon coating using an Emitech K 950 carbon evaporator. Thermogravimetric analysis (TGA) was performed using a Shimadzu TGA-50 system at a heating rate of 5 ºC min^{-1} under air. FT-IR spectra were obtained as KBr pellets using a FTIR Mattson-7000 spectrophotometer and recorded in transmission mode from 4000 to 300 cm^{-1} with a resolution of 4 cm^{-1}. Raman spectra were recorded on a Bruker RFS100/S FT instrument (Nd:YAG laser, 1064 nm excitation, InGaAs detector). Solid-state $^{13}C\{^1H\}$ cross-polarization (CP) magic-angle spinning (MAS) NMR spectra were recorded at 100.62 MHz on a Bruker Avance 400 spectrometer using 3.5 μs ^1H 90º pulses, a 2 ms

contact time, a spinning rate of 10 kHz, and 5 s recycle delays. Chemicals shifts are quoted in ppm relative to TMS.

Photophysical characterization

UV-Vis and fluorescence spectra were recorded with Cary 5000 UV-Vis-NIR and Horiba-Jobin-Ivon SPEX FluoroLog 3–22 spectrophotometers, respectively. For solution samples, dimethylsulfoxide (DMSO) was of spectroscopic or equivalent grade and was used as received. The water was Milli-Q grade. For solid samples, the absorption spectra were recorded by diffuse reflectance using the Cary 5000 UV-Vis-NIR spectrophotometer equipped with an integrating sphere. Before spectra of solid samples were recorded, a baseline, with barium sulfate, was obtained. Fluorescence spectra were corrected for the wavelength response of the system. The FluoroLog spectrophotometer consists of a modular spectrofluorimeter with double grating excitation (range 200-950 nm, optimized in the UV and with a blazed angle at 330 nm) and emission (range 200-950 nm, optimized in the visible and with a blazed angle at 500 nm) monochromators. The bandpass for excitation and emission is 0–15 nm (values that are continuously adjustable using computer Datamax/32 software) and the wavelength accuracy is ±0.5 nm. The excitation source consists of an ozone-free 450 W Xenon lamp and the emission detector is a Hamamatsu R928 Photomultiplier (200-950 nm range), cooled with a Products for Research thermoelectric refrigerated chamber (model PC177CE005), or a Hamamatsu R5509-42 (900-1400 nm range), cooled to 193 K in a liquid nitrogen chamber (Products for Research model PC176TSCE-005), and a photodiode as the reference detector.[78] The solid-state fluorescence spectra were obtained using triangular quartz cuvettes.

For solution samples, fluorescence quantum yields (ϕ_F) were determined by comparison with references of known quantum yield. The emission quantum yields of these standards should be independent of the excitation wavelength, so the standards can be used in their full absorption range. In practice the quantum yields are determined by comparison of the integrated area under the emission spectra of optically matched solutions of the sample compound (*cp*) ($\int I(\lambda)^{cp} d\lambda$) and that of the suitable reference (*ref*) compound ($\int I(\lambda)^{ref} d\lambda$). The absorption and emission range of the sample and reference compounds should match as close as possible. The absorbance values should be kept as low as possible to avoid inner filter effects (usually with A < 0.2). Under these conditions, using the same excitation wavelength, the unknown fluorescence quantum yield (ϕ_F^{cp}) is calculated using Equation 1,[79]

$$J \quad (1)$$

where n_x is the refractive index of the solvent in which the sample compound and reference were dissolved, and OD_x is the optical density of the reference and sample compound at the excitation wavelength. The fluorescence standards (references) used were α-oligothiophene α6 (ϕ_F = 0.41 in dioxane[80]) for CR in water, and cresyl violet (ϕ_F = 0.54 in ethanol[81]) for CR in DMSO.

For the titration of CR, a solution of the dye in water (pH 6.3) was prepared with an absorbance below 0.2 at 497 nm. The pH was adjusted by addition of HCl and NaOH solutions (0.1 and 1 M).

The experimental setup for ultrafast spectroscopic and kinetic measurements [femtosecond time-resolved transient absorption (fs-TA) spectroscopy] was described previously.[82] It basically consists of a broadband (350-1600 nm) HELIOS pump-probe fs-TA spectrometer from Ultrafast Systems, equipped with an amplified femtosecond Spectra-Physics Solstice-100F laser (displaying a pulse width of 128 fs and 1 kHz repetition rate) coupled with a Spectra-Physics TOPAS Prime F optical parametric amplifier (195-22000 nm) for pulse pump generation. Probe light in the Vis range was generated by passing a small portion of the 795 nm light from the Solstice-100F laser through a computerized optical delay (with a time window of up to 8 ns) and focusing in a sapphire plate to generate white-light continuum in the 450-800 nm range. All measurements were obtained in a 2 mm quartz cuvette with absorptions ≤0.3 at the pump excitation wavelength, and to avoid multiphoton absorption the laser pump power was kept at ≤0.5 μJ. The instrumental response function (IRF) of the system was assumed to be equal to that of the pump-probe cross correlation determined from the measurement of the instantaneous stimulated Raman signal from the pure solvent (in a 2 mm cuvette). Typical values for the IRF of the system were found to be better than 250 fs. To avoid photodegradation the solutions were stirred during the experiments or in movement using a motorized translating sample holder. Transient absorption data were analyzed using the Surface Xplorer PRO program from Ultrafast Systems and the global analysis of the data (from which the lifetimes and decay associated spectra, DAS, of the observed transients were obtained) was performed using Glotaran software.[83] Further details about the global analysis of the data (including singular value decomposition) and the interpretation of the resulting outputs (DAS and concentration profiles) can be found in reference [83].

Materials and synthesis

Starting materials. $Zn(NO_3)_2 \cdot 6H_2O$ (Fluka), $Al(NO_3)_3 \cdot 9H_2O$ (Riedel-de-Haën), 1 M NaOH (Fluka) and acetone (99.5%, Sigma-Aldrich) were obtained from commercial sources and used as received. All LDH preparations were performed under nitrogen using deionized and decarbonated (DD) water. Congo Red (CR) [sodium salt of 3,3'-([1,1'-biphenyl]-4,4'-diyl)bis(4-aminonaphthalene-1-sulfonic acid) was obtained from BDH Chemicals and recrystallized from water-ethanol (1:1) before use.

Synthesis of NO_3-LDH. For reference, a nitrate-form Zn-Al LDH was prepared by using the standard method of coprecipitation of the Zn^{2+} and Al^{3+} hydroxides (initial Zn^{2+}/Al^{3+} molar ratio in solution = 2) in the presence of nitrate ions at constant pH (7.5–8) under nitrogen, followed by aging of the gel at 80 °C for 20 h.[84] Anal. Calcd for $[Zn_4Al_2(OH)_{12}][(NO_3)_2(H_2O)_{2.5}]$ (688.7): H, 2.49; N, 4.07. Found: H, 2.26; N, 4.12%. TGA showed a mass loss of 7.0% up to 150 ºC (calcd, for loss of $2.5H_2O$: 6.5%), and a residual mass of 64.6% at 700 ºC (calcd, for $Zn_4Al_2O_7$: 62.1%). FT-IR (KBr, cm^{-1}): ν = 3448 (br), 2925 (w), 1624 (br), 1385 (vs), 1018 (w), 825 (w), 613 (m), 555 (sh), 426 (vs), 314 (m). Raman (cm^{-1}): ν = 3420, 1389, 1055, 716, 550, 489, 114.

Synthesis of CR-LDH. A solution of $Zn(NO_3)_2 \cdot 6H_2O$ (1.49 g, 5 mmol) and $Al(NO_3)_3 \cdot 9H_2O$ (0.94 g, 2.5 mmol) in DD water (30 mL) was added dropwise to a solution of CR (1.74 g, 2.5 mmol) in DD water (150 mL) with efficient mixing. The pH of the reaction mixture was maintained at 7.5-8 by simultaneous addition of 0.5 M NaOH. Once addition of the Zn^{2+}/Al^{3+} solution was complete, the resultant red gel-like slurry (pH 7.5-8) was stirred for 18 h at 65 °C. The dark red solid was isolated by filtration, washed several times with DD water and acetone (4 × 50 mL), and finally dried at room temperature under reduced pressure in a vacuum desiccator. Anal. Calcd for $[Zn_4Al_2(OH)_{12}][(C_{32}H_{22}N_6O_6S_2)_{0.86}(CO_3)_{0.14}(H_2O)_7]$ (1213.7): C, 27.37; H, 3.73; N, 5.95; S, 4.54. Found: C, 27.54; H, 3.61; N, 5.86; S, 4.40%. TGA showed a mass loss of 10.2% up to 200 ºC (calcd, for loss $7H_2O$: 10.4%), and a residual mass of 35.8% at 800 ºC (calcd, for $Zn_4Al_2O_7$: 35.2%). FT-

IR (KBr, cm^{-1}): ν = 3426 (br), 2964 (w), 2923 (w), 2854 (w), 1612 (s), 1508 (w), 1448 (w), 1431 (w), 1375 (m), 1261 (m), 1225 (w), 1174 [s, $\nu_{as}(SO_3^-)$], 1105 (m), 1043 [s, $\nu_s(SO_3^-)$], 947 (w), 914 (w), 858 (w), 802 (s), 831 (m), 756 (m), 721 (w), 696 (m), 669 (m), 624 (m), 596 (m), 536 (w), 462 (w), 424 (m). Raman (cm^{-1}): ν = 3394 (br), 1590 (vs), 1451 (m), 1433 (m), 1373 (vs), 1325 (m), 1281 (m), 1248 (w), 1211, 1151 (vs), 1040 (w), 942 (w), 408 (w), 359 (w). $^{13}C\{^1H\}$ CP MAS NMR: δ = 149.9 (C^1), 138.8 (C^{10}), 137.0 (C^4), 126.5 ($C^{14,13,8,7,5,3}$), 124.3 ($C^{12,11,9,2}$), 115.0 (C^6) (see Figure 10 for the atom numbering scheme).

Acknowledgements

We acknowledge funding by FEDER (Fundo Europeu de Desenvolvimento Regional) through COMPETE (Programa Operacional Factores de Competitividade). National funding through the FCT (Fundação para a Ciência e a Tecnologia) within the projects Coimbra Chemistry Centre (PEst-OE/QUI/UI0313/2014) and FCOMP-01-0124-FEDER-029779 (FCT ref. PTDC/QEQ-SUP/1906/2012) is thanked. This work was developed within the scope of the project CICECO-Aveiro Institute of Materials, POCI-01-0145-FEDER-007679 (FCT Ref. UID/CTM/50011/2013), financed by national funds through the FCT/MEC and when appropriate co-financed by FEDER under the PT2020 Partnership Agreement. The FCT is acknowledged for a PhD grant to A.L.C. (ref. SFRH/BD/88806/2012) and post-doctoral grants to A.C.G. (ref. SFRH/BPD/108541/2015) and J.P. (ref. SFRH/BPD/108469/2015).

Keywords: Congo Red • Layered double hydroxides • Intercalations • Aggregation • Photophysics

[1] B. Heyne, *Photochem. Photobiol. Sci.* **2016**, *15*, 1103-1114.
[2] Z. Chen, A. Lohr, C.R. Saha-Möller, F. Würthner, *Chem. Soc. Rev.* **2009**, *38*, 564-584.
[3] F. Würthner, T.E. Kaiser, C.R. Saha-Möller, *Angew. Chem. Int. Ed.* **2011**, *50*, 3376-3410.
[4] D. Möbius, *Adv. Mater.* **1995**, *7*, 437-444.
[5] H.B. Rodríguez, E.S. Román, *Photochem. Photobiol.* **2013**, *89*, 1273-1282.
[6] C.-T. Chen, *Chem. Mater.* **2004**, *16*, 4389-4400.
[7] J. Mei, N.L.C. Leung, R.T.K. Kwok, J.W.Y. Lam, B.Z. Tang, *Chem. Rev.* **2015**, *115*, 11718-11940.
[8] M. Gsänger, D. Bialas, L. Huang, M. Stolte, F. Würthner, *Adv. Mater.* **2016**, *28*, 3615-3645.
[9] R. Pardo, M. Zayat, D. Levy, *Chem. Soc. Rev.* **2011**, *40*, 672-687.
[10] B. Lebeau, P. Innocenzi, *Chem. Soc. Rev.* **2011**, *40*, 886-906.
[11] L. Latterini, N. Nocchetti, G.G. Aloisi, U. Costantino, F. Elisei, *Inorg. Chim. Acta* **2007**, *360*, 728-740.
[12] D. Yan, J. Lu, M. Wei, D.G. Evans, X. Duan, *J. Mater. Chem.* **2011**, *21*, 13128-13139.
[13] E. Merino, *Chem. Soc. Rev.* **2011**, *40*, 3835-3853.
[14] K. Hunger, Industrial Dyes: Chemistry, Properties, Applications, Wiley-VCH, Weinheim, Germany, **2003**.
[15] H.M.D. Bandara, S.C. Burdette, *Chem. Soc. Rev.* **2012**, *41*, 1809-1825.
[16] M. Han, S.J. Cho, Y. Norikane, M. Shimizu, A. Kimura, T. Tamagawa, T. Seki, *Chem. Commun.* **2014**, *50*, 15815-15818.
[17] P. Spólnik, M. Król, B. Stopa, L. Konieczny, B. Piekarska, J. Rybarska, G. Zemanek, A. Jagusiak, P. Piwowar, G. Szoniec, I. Roterman, *Eur. Biophys. J.* **2011**, *40*, 1187-1196.
[18] M. Skowronek, B. Stopa, L. Konieczny, J. Rybarska, B. Piekarska, E. Szneler, G. Bakalarski, I. Roterman, *Biopolymers* **1998**, *46*, 267-281.
[19] B. Stopa, A. Jagusiak, L. Konieczny, B. Piekarska, J. Rybarska, G. Zemanek, M. Król, P. Piwowar, I. Roterman, *J. Mol. Model.* **2013**, *19*, 4731-4740.
[20] T. Panczyk, P. Wolski, A. Jagusiak, M. Drach, RSC Adv. **2014**, *4*, 47304-47312.
[21] B. Neumann, P. Pollmann, *Phys. Chem. Chem. Phys.* **2001**, *3*, 4508-4514.
[22] P. Frid, S.V. Anisimov, N. Popovic, *Brain Res. Rev.* **2007**, *53*, 135-160.
[23] C. Lendel, B. Bolognesi, A. Wahlström, C.M. Dobson, A. Gräslund, *Biochem.* **2010**, *49*, 1358-1360.
[24] A.J. Howie, D.B. Brewer, *Micron* **2009**, *40*, 285-301.
[25] C. Wu, J. Scott, J.E. Shea, *Biophys. J.* **2012**, *103*, 550-557.
[26] T.M. Cooper, M.O. Stone, *Langmuir* **1998**, *14*, 6662-6668.
[27] H. Yamamoto, A. Nakazawa, T. Hayakawa, *J. Polym. Sci.: Polym. Lett. Ed.* **1983**, *21*, 131-138.
[28] R.A. Edwards, R.W. Woody, *Biochem.* **1979**, *18*, 5197-5204.
[29] D.N. de Vasconcelos, V.F. Ximenes, *Spectrochim. Acta A: Mol. Biomol. Spectrosc.* **2015**, *150*, 321-330.
[30] S.B. Yamaki, D.S. Barros, C.M. Garcia, P. Socoloski, O.N. Oliveira Jr, T.D.Z. Atvars, *Langmuir* **2005**, *21*, 5414-5420.
[31] C.-F. Mao, M.-C. Hsu, W.-H. Hwang, *Carbohydrate Polym.* **2007**, *68*, 502-510.
[32] E. Katmiwati, T. Nakanishi, *Macromol. Res.* **2014**, *22*, 731-737.
[33] J. Barkauskas, J. Dakševič, R. Juškėnas, R. Mažeikienė, G. Niaura, G. Račiukaitis, A. Selskis, I. Stankevičienė, R. Trusovas, *J. Mater. Sci.* **2012**, *47*, 5852-5860.
[34] K. Ariga, Y. Lvov, T. Kunitake, *J. Am. Chem. Soc.* **1997**, *119*, 2224-2231.
[35] J.-A. He, S. Bian, L. Li, J. Kumar, S.K. Tripathy, L.A. Samuelson, *J. Phys. Chem. B* **2000**, *104*, 10513-10521.
[36] X. Tao, J. Li, H. Möhwald, *Chem. Eur. J.* **2004**, *10*, 3397-3403.
[37] J. Kurczewska, G. Schroeder, *Cent. Eur. J. Chem.* **2011**, *9*, 41-46.
[38] B. Onida, B. Bonelli, L. Flora, F. Geobaldo, C.O. Arean, E. Garrone, *Chem. Commun.* **2001**, 2216-2217.
[39] L. Borello, B. Onida, C. Barolo, K.J. Edler, C.O. Areán, E. Garrone, *Sensor. Actuat. B: Chem.* **2004**, *100*, 107-111.
[40] P. Rivolo, P. Pirasteh, A. Chaillou, P. Joubert, M. Kloul, J.-F. Bardeau, F. Geobaldo, *Sensor. Actuat. B: Chem.* **2004**, *100*, 99-102.
[41] F.A. Pavan, E.S. Ribeiro, Y. Gushikem, *Electroanal.* **2005**, *17*, 625-629.
[42] A. Chouket, B. Cherif, N. Ben Salah, K. Khirouni, *J. Appl. Phys.* **2013**, *114*, article no. 243105.
[43] B. Wu, W.-H. Zhang, Z.-G. Ren, J.-P. Lang, *Chem. Commun.* **2015**, *51*, 14893-14896.
[44] A. Gültek, Y. Gökçen, S. Köytepe, T. Seçkin, *Macromol. Symp.* **2010**, *296*, 92-99.
[45] B. Hu, F. Dai, Z. Fan, G. Ma, Q. Tang, X. Zhang, *Adv. Mater.* **2015**, *27*, 5499-5505.
[46] M.O. Iwunze, *Spectros. Lett.* **2010**, *43*, 16-21.
[47] S.J. Strickler, R.A. Berg, *J. Chem. Phys.* **1962**, *37*, 814-822.
[48] F. Márquez, M.J. Sabater, *J. Phys. Chem. B* **2005**, *109*, 16593-16597.
[49] K. Yokoyama, A. Fisher, A. Amori, D. Welchons, R. McKnight, *J. Biophys. Chem.* **2010**, *3*, 153-163.
[50] M. Kasha, *Energy Radiat. Res.* **2012**, *178*, AV27-AV34.
[51] M. Kasha, H. Rawls, M. El-Bayoumi, *Pure Appl. Chem.* **1965**, *11*, 371-392.
[52] P. Douglas, H.D. Burrows, R.C. Evans, Foundations of Photochemistry: A Background on the Interaction Between Light and Molecules, in *Applied Photochemistry* (Eds.: C.R. Evans, P. Douglas, D.H. Burrow), Springer Netherlands, Dordrecht, **2013**, pp. 1-88.
[53] T. James, *The Theory of the Photographic Process*, 3rd ed., Macmillan, New York, **1966**.
[54] J.C. Dean, D.G. Oblinsky, S. Rafiq, G.D. Scholes, *J. Phys. Chem. B* **2016**, *120*, 440-454.

[55] Y. Deng, W. Yuan, Z. Jia, G. Liu, *J. Phys. Chem. B* **2014**, *118*, 14536-14545.

[56] J. Bujdák, N. Iyi, *J. Colloid Interface Sci.* **2008**, *326*, 426-432.

[57] *J-Aggregates* (Ed.: T. Kobayashi), World Scientific Publishing Co. Pte. Ltd., Singapore, **2012**.

[58] G. Cui, P.-J. Guan, W.-H. Fang, *J. Phys. Chem. A* **2014**, *118*, 4732-4739.

[59] R.S. Becker, *Theory and Interpretation of Fluorescence and Phosphorescence*, Wiley-Interscience, New York, **1969**.

[60] N. Turro, *Modern Molecular Photochemistry*, University Science Books, Sausalito, California, **1991**.

[61] E. Pigorsch, A. Elhaddaoui, S. Turrell, *Spectrochim. Acta A: Mol. Biomol. Spectrosc.* **1994**, *50*, 2145-2152.

[62] M.L. Horng, J.A. Gardecki, A. Papazyan, M. Maroncelli, *J. Phys. Chem.* **1995**, *99*, 17311-17337.

[63] R.M. Stratt, M. Maroncelli, *J. Phys. Chem.* **1996**, *100*, 12981-12996.

[64] U. Costantino, N. Coletti, M. Nocchetti, G.G. Aloisi, F. Elisei, *Langmuir* **1999**, *15*, 4454-4460.

[65] N. Iyi, K. Kurashima, T. Fujita, *Chem. Mater.* **2002**, *14*, 583-589.

[66] G. Abellán, E. Coronado, C. Martí-Gastaldo, A. Ribera, J.L. Jordá, H. García, Adv. Mater. **2014**, *26*, 4156-4162.

[67] W.H. Ojala, C.R. Ojala, W.B. Gleason, Antivir. *Chem. Chemoth.* **1995**, *6*, 25-33.

[68] F.A. Rad, Z. Rezvani, F. Khodam, *RSC Adv.* **2016**, *6*, 11193-11203.

[69] D.P. Yan, Y.B. Zhao, M. Wei, R.Z. Liang, J. Lu, D.G. Evans, X. Duan, *RSC Adv.* **2013**, *3*, 4303-4310.

[70] K. Adachi, K. Watanabe, S. Yamazaki, *Ind. Eng. Chem. Res.* **2014**, *53*, 13046-13057.

[71] J. Bauer, P. Behrens, M. Speckbacher, H. Langhals, *Adv. Funct. Mater.* **2003**, *13*, 241-248.

[72] D. Yan, J. Lu, M. Wei, J. Ma, D.G. Evans, X. Duan, *Phys. Chem. Chem. Phys.* **2009**, *11*, 9200-9209.

[73] S. Gago, T. Costa, J. Seixas de Melo, I.S. Goncalves, M. Pillinger, *J. Mater. Chem*. **2008**, *18*, 894-904.

[74] A.L. Costa, A.C. Gomes, M. Pillinger, I.S. Goncalves, J.S. Seixas de Melo, *Chem. Eur. J.* **2015**, *21*, 12069-12078.

[75] J. Wang, X.M. Ren, X.S. Feng, S.Y. Liu, D.J. Sun, *J. Colloid Interface Sci.* **2008**, *318*, 337-347.

[76] T. Miura, C. Yamamiya, M. Sasaki, K. Suzuki, H. Takeuchi, *J. Raman Spectros.* **2002**, *33*, 530-535.

[77] E. McRae, M. Kasha, *The Molecular Exciton Model*, in *Physical Processes in Radiation Biology*, Academic Press, New York, **1964**.

[78] J.S. Seixas de Melo, T. Costa, A. Francisco, A.L. Macanita, S. Gago, I.S. Goncalves, *Phys. Chem. Chem. Phys.* **2007**, *9*, 1370-1385.

[79] S. Murov, I. Carmichael, G. Hug, *Handbook of Photochemistry*, 2nd ed., Marcel Dekker, Inc., New York, **1993**.

[80] R.S. Becker, J. Seixas de Melo, A.L. Macanita, F. Elisei, *J. Phys. Chem.* **1996**, *100*, 18683-18695.

[81] M. Montalti, A. Credi, L. Prodi, M. Gandolfi, *Handbook of Photochemistry*, 3rd ed., CRC Press, Boca Raton, **2006**.

[82] J. Pina, J.S. Seixas de Melo, A. Eckert, U. Scherf, *J. Mater. Chem. A* **2015**, *3*, 6373-6382.

[83] J.J. Snellenburg, S.P. Laptenok, R. Seger, K.M. Mullen, I.H.M. van Stokkum, *J. Stat. Soft.* **2012**, *49*, 1-22.

[84] A.C. Gomes, S.M. Bruno, C.A. Gamelas, A.A. Valente, M. Abrantes, I.S. Goncalves, C.C. Romao, M. Pillinger, *Dalton Trans.* **2013**, *42*, 8231-8240.

Entry for the Table of Contents

ARTICLE

The self-assembly of the anionic diazo dye Congo Red (CR) in the solid state was investigated by intercalating the dye in a layered double hydroxide and characterizing the resultant hybrid material by various techniques. In combination with a deep analysis of the photophysics of CR in solution, the results point towards the presence of slipped cofacial J-type aggregates in the hybrid material, giving rise to the exceptionally large basal spacing of 26.2 Å (see picture).

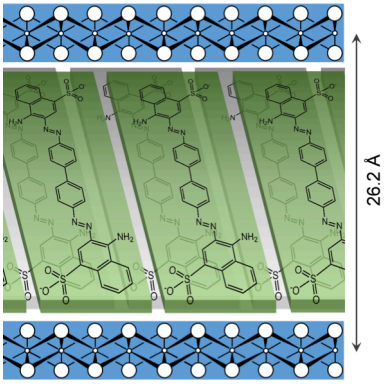

Ana L. Costa, Ana C. Gomes, Martyn Pillinger, Isabel S. Gonçalves, João Pina, and J. Sérgio Seixas de Melo**

Page No. – Page No.

Comprehensive investigation of the photophysics and supramolecular organisation of Congo Red in solution, the solid state, and intercalated in a layered double hydroxide